

Stochastic Multiple Target Sampling Gradient Descent

Hoang Phan[◇] Ngoc N. Tran[◇] Trung Le[†] Toan Tran[◇] Nhat Ho[‡] Dinh Phung[†]
Monash University, Australia[†]; VinAI Research[◇]; University of Texas, Austin[‡]

September 26, 2022

Abstract

Sampling from an unnormalized target distribution is an essential problem with many applications in probabilistic inference. Stein Variational Gradient Descent (SVGD) has been shown to be a powerful method that iteratively updates a set of particles to approximate the distribution of interest. Furthermore, when analysing its asymptotic properties, SVGD reduces exactly to a single-objective optimization problem and can be viewed as a probabilistic version of this single-objective optimization problem. A natural question then arises: “*Can we derive a probabilistic version of the multi-objective optimization?*”. To answer this question, we propose *Stochastic Multiple Target Sampling Gradient Descent* (MT-SGD), enabling us to sample from multiple unnormalized target distributions. Specifically, our MT-SGD conducts a flow of intermediate distributions gradually orienting to multiple target distributions, which allows the sampled particles to move to the joint high-likelihood region of the target distributions. Interestingly, the asymptotic analysis shows that our approach reduces exactly to the multiple-gradient descent algorithm for multi-objective optimization, as expected. Finally, we conduct comprehensive experiments to demonstrate the merit of our approach to multi-task learning.

1 Introduction

Sampling from an unnormalized target distribution that we know the density function up to a scaling factor is a pivotal problem with many applications in probabilistic inference [2, 20, 29]. For this purpose, Markov chain Monte Carlo (MCMC) has been widely used to draw approximate posterior samples, but unfortunately, is often time-consuming and has difficulty accessing the convergence [16]. Targeting an efficient acceleration of MCMC, some stochastic variational particle-based approaches have been proposed, notably Stochastic Langevin Gradient Descent [30] and Stein Variational Gradient Descent (SVGD) [16]. Outstanding among them is SVGD, with a solid theoretical guarantee of the convergence of the set of particles to the target distribution by maintaining a flow of distributions. More specifically, SVGD starts from an arbitrary and easy-to-sample initial distribution and learns the subsequent distribution in the flow by push-forwarding the current one using a function $T(x) = x + \epsilon \phi(x)$, where $x \in \mathbb{R}^d$, $\epsilon > 0$ is the learning rate, and $\phi \in \mathcal{H}_k^d$ with \mathcal{H}_k to be the Reproducing Kernel Hilbert Space corresponding to a kernel k . It is well-known that for the case of using Gaussian RBF kernel, by letting the kernel width approach $+\infty$, the update formula of SVGD at each step asymptotically reduces to the typical gradient descent (GD) [16], showing the connection between a probabilistic framework like SVGD and a single-objective optimization algorithm. In other words, SVGD can be viewed as a probabilistic version of the GD for single-objective optimization.

On the other side, multi-objective optimization (MOO) [8] aims to optimize a set of objective functions and manifests itself in many real-world applications problems, such as in multi-task learning (MTL) [19, 27], natural language processing [1], and reinforcement learning [10, 25, 24]. Leveraging the above insights, it is natural to ask: “*Can we derive a probabilistic version of multi-objective*

optimization? By answering this question, we enable the application of the Bayesian inference framework to the tasks inherently fulfilled by the MOO framework.

Contribution. In this paper, we provide an affirmative answer to that question. In particular, we go beyond the SVGD to propose *Stochastic Multiple Target Sampling Gradient Descent* (MT-SGD), enabling us to sample from multiple target distributions. By considering the push-forward map $T(x) = x + \epsilon\phi(x)$ with $\phi \in \mathcal{H}_k^d$, we can find a closed-form for the optimal push-forward map T^* pushing the current distribution on the flow simultaneously closer to all target distributions. Similar to SVGD, in the case of using Gaussian RBF kernel, when the kernel width approaches $+\infty$, MT-SGD reduces exactly to the multiple-gradient descent algorithm (MGDA) [8] for multi-objective optimization (MOO). Our MT-SGD, therefore, can be considered as a probabilistic version of the GD multi-objective optimization [8] as expected.

Additionally, in practice, we consider a flow of discrete distributions, in which, each distribution is presented as a set of particles. Our observations indicate that MT-SGD globally drives the particles to close to all target distributions, leading them to diversify on the *joint high-likelihood region* for all distributions. It is worth noting that, different from other multi-particle approaches [15, 17, 19] leading the particles to diversify on a Pareto front, our MT-SGD orients the particle to diversify on the so-called *Pareto common* (i.e., the joint high-likelihood region for all distributions) (cf. Section 2.4 for more discussions). We argue and empirically demonstrate that this characteristic is essential for the Bayesian setting, whose main goal is to estimate the *ensemble accuracy* and the *uncertainty calibration* of a model. In summary, we make the following contributions in this work:

- Propose a principled framework that incorporates the power of Stein Variational Gradient Descent into multi-objective optimization. Concretely, our method is motivated by the theoretical analysis of SVGD, and we further derive the formulation that extends the original work and allows to sample from multiple unnormalize distributions.
- Demonstrate our algorithm is readily applicable in the context of multi-task learning. The benefits of MT-SGD are twofold: i) the trained network is optimal, which could not be improved in any task without diminishing another, and ii) there is no need for predefined preference vectors as in previous works [15, 19], MT-SGD implicitly learns diverse models universally optimizing for all tasks.
- Conduct comprehensive experiments to verify the behaviors of MT-SGD and demonstrate the superiority of MT-SGD to the baselines in a Bayesian setting, with higher ensemble performances and significantly lower calibration errors.

Related works. The work of [8] proposed a multi-gradient descent algorithm for multi-objective optimization (MOO) which opens the door for the applications of MOO in machine learning and deep learning. Inspired by [8], MOO has been applied in multi-task learning (MTL) [19, 27], few-shot learning [5, 32], and knowledge distillation [6, 9]. Specifically, in an earlier attempt at solving MTL, [27] viewed multi-task learning as a multi-objective optimization problem, where a task network consists of a shared feature extractor and a task-specific predictor. In another study, [19] developed a gradient-based multi-objective MTL algorithm to find a set of solutions that satisfies the user preferences. Also follows the idea of learning neural networks conditioned on pre-defined preference vectors, [15] proposed Pareto MTL, aiming to find a set of well-distributed Pareto solutions, which can represent different trade-offs among different tasks. Recently, the work of [17] leveraged MOO with SVGD [16] and Langevin dynamics [30] to diversify the solutions of MOO. In another line

of work, [32] proposed a bi-level MOO that can be applied to few-shot learning. Furthermore, a somewhat different result was proposed, [9] applied MOO to enable the knowledge distillation from multiple teachers and find a better optimization direction in training the student network.

Outline. The paper is organized as follows. In Section 2, we first present our theoretical contribution by reviewing the formalism and providing the point of view adopted to generalize SVGD in the context of MOO. Then, Section 3 introduces an algorithm to showcase the application of our proposed method in the multi-task learning scenario. We report the results of extensive experimental studies performed on various datasets that demonstrate the behaviors and efficiency of MT-SGD in Section 4. Finally, we conclude the paper in Section 5. The complete proofs and experiment setups are deferred to the supplementary material.

2 Multi-Target Sampling Gradient Descent

We first briefly introduce the formulation of the multi-target sampling in Section 2.1. Second, Section 2.2 presents our theoretical development and shows how our proposed method is applicable to this problem. Finally, we detail how to train the proposed method in Section 2.3 and highlight key differences between our method and related work in Section 2.4.

2.1 Problem Setting

Given a set of target distributions $p_{1:K}(\theta) := \{p_1(\theta), \dots, p_K(\theta)\}$ with parameter $\theta \in \mathbb{R}^d$, we aim to find the optimal distribution $q^* \in \mathcal{Q}$ that minimizes a vector-valued objective function whose k -th component is $D_{KL}(q\|p_k)$:

$$\min_{q \in \mathcal{Q}} [D_{KL}(q\|p_1), \dots, D_{KL}(q\|p_K)], \quad (1)$$

where D_{KL} represents Kullback-Leibler divergence and \mathcal{Q} is a family of distributions.

When there exists an objective function that conflicts with each other, there will be a trade-off between these two objectives. Therefore, no “optimal solution” exists in such cases. Alternatively, we are often interested in seeking a set of solutions such that each does not have any better solution (i.e. achieves lower loss values in all objectives) [15, 17, 27]. The optimization problem (OP) in (1) thus can be viewed as a multi-objective OP [8] on the probability distribution space. Let us denote \mathcal{H}_k by the Reproducing Kernel Hilbert Space (RKHS) associated with a positive semi-definite (p.s.d.) kernel k , and \mathcal{H}_k^d by the d -dimensional vector function:

$$f = [f_1, \dots, f_d], (f_i \in \mathcal{H}_k).$$

Inspired by [16], we construct a flow of distributions q_0, q_1, \dots, q_L departed from a simple distribution q_0 , that gradually move closer to all the target distributions. In particular, at each step, assume that q is the current obtained distribution, and the goal is to learn a transformation $T = id + \epsilon\phi$ so that the *feed-forward distribution* $q^{[T]} = T\#q$ moves closer to $p_{1:K}$ simultaneously. Here we use id to denote the identity operator, $\epsilon > 0$ is a step size, and $\phi \in \mathcal{H}_k^d$ is a velocity field. Particularly, the problem of finding the optimal transformation T for the current step is formulated as:

$$\min_{\phi} [D_{KL}(q^{[T]}\|p_1), \dots, D_{KL}(q^{[T]}\|p_K)]. \quad (2)$$

2.2 Our Theoretical Development

It is worth noting that the transformation T defined above is injective when ϵ is sufficiently small [16]. We consider each $D_{KL}(q^{[T]} \| p_i)$, $i = 1, \dots, K$ as a function w.r.t. ϵ , by applying the first-order Taylor expansion at 0, we have:

$$D_{KL}(q^{[T]} \| p_i) = D_{KL}(q \| p_i) + \nabla_{\epsilon} D_{KL}(q^{[T]} \| p_i) \Big|_{\epsilon=0} \epsilon + O(\epsilon^2),$$

where $\lim_{\epsilon \rightarrow 0} O(\epsilon^2) / \epsilon^2 = \text{const.}$

Given that the velocity field $\phi \in \mathcal{H}_k^d$, similar to [16], the gradient $\nabla_{\epsilon} D_{KL}(q^{[T]} \| p_i) \Big|_{\epsilon=0}$ can be calculated as provided in ¹

$$\nabla_{\epsilon} D_{KL}(q^{[T]} \| p_i) \Big|_{\epsilon=0} = -\langle \phi, \psi_i \rangle_{\mathcal{H}_k^d},$$

where $\psi_i(\cdot) = \mathbb{E}_{\theta \sim q}[k(\theta, \cdot) \nabla_{\theta} \log p_i(\theta) + \nabla_{\theta} k(\theta, \cdot)]$ and $\langle \cdot, \cdot \rangle_{\mathcal{H}_k^d}$ is the dot product in the RKHS.

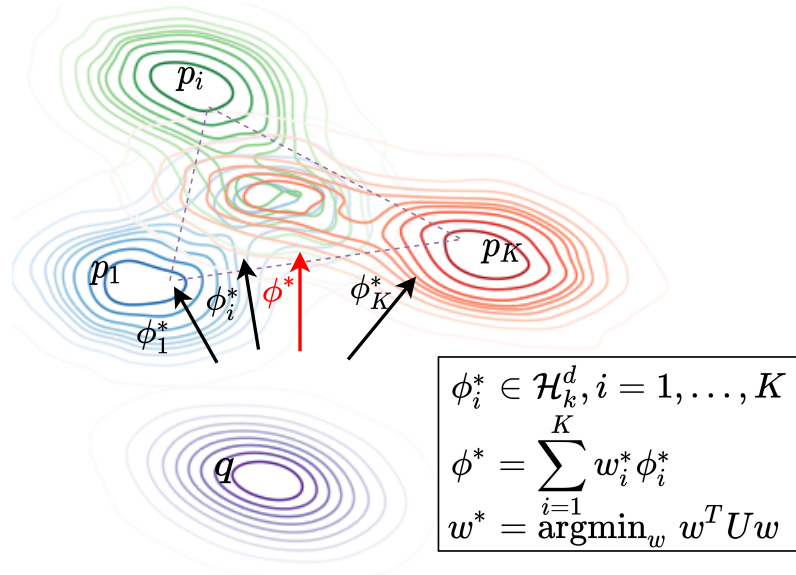


Figure 1: How to find the optimal descent direction ϕ^* .

This means that, for each target distribution p_i , the steepest descent direction is $\phi_i^* = \psi_i$, in which the KL divergence of interest $D_{KL}(q^{[T]} \| p_i)$ gets decreased roughly by $-\epsilon \|\phi_i^*\|_{\mathcal{H}_k^d}^2$ toward the target distribution p_i . However, this only guarantees a divergence reduction for a single target distribution p_i itself. Our next aim is hence to find a common direction ϕ^* to reduce the KL divergences w.r.t. all target distributions, which is reflected in the following lemma, showing us how to combine the individual steepest descent direction $\phi_i^* = \psi_i$ to yield the optimal direction ϕ^* as summarized in Figure 1.

Lemma 1. Let w^* be the optimal solution of the optimization problem $w^* = \underset{w \in \Delta_K}{\operatorname{argmin}} w^T U w$ and $\phi^* = \sum_{i=1}^K w_i^* \phi_i^*$, where $\Delta_K = \{\pi \in \mathbb{R}_+^K : \|\pi\|_1 = 1\}$ and $U \in \mathbb{R}^{K \times K}$ with $U_{ij} = \langle \phi_i^*, \phi_j^* \rangle_{\mathcal{H}_k^d}$, then we have

$$\langle \phi^*, \phi_i^* \rangle_{\mathcal{H}_k^d} \geq \|\phi^*\|_{\mathcal{H}_k^d}^2, i = 1, \dots, K.$$

Lemma 1 provides a common descent direction ϕ^* so that all KL divergences w.r.t. the target distributions are consistently reduced by $\epsilon \|\phi^*\|_{\mathcal{H}_k^d}^2$ roughly and Theorem 2 confirms this argument.

Theorem 2. *If there does not exist $w \in \Delta_K$ such that $\sum_{i=1}^K w_i \phi_i^* = 0$, given a sufficiently small step size ϵ , all KL divergences w.r.t. the target distributions are strictly decreased by at least $A \|\phi^*\|_{\mathcal{H}_k^d}^2 > 0$ where A is a positive constant.*

The next arising question is how to evaluate the matrix $U \in \mathbb{R}^{K \times K}$ with $U_{ij} = \langle \phi_i^*, \phi_j^* \rangle_{\mathcal{H}_k^d}$ for solving the quadratic problem: $\min_{w \in \Delta_K} w^T U w$. To this end, using some well-known equalities in the RKHS¹, we arrive at the following formula:

$$U_{ij} = \langle \phi_i^*, \phi_j^* \rangle_{\mathcal{H}_k^d} = \mathbb{E}_{\theta, \theta' \sim q} \left[k(\theta, \theta') \langle \nabla \log p_i(\theta), \nabla \log p_j(\theta') \rangle + \left\langle \nabla \log p_i(\theta), \frac{\partial k(\theta, \theta')}{\partial \theta'} \right\rangle + \left\langle \nabla \log p_j(\theta'), \frac{\partial k(\theta, \theta')}{\partial \theta} \right\rangle + \text{tr} \left(\frac{\partial^2 k(\theta, \theta')}{\partial \theta \partial \theta'} \right) \right], \quad (3)$$

where $\text{tr}(\cdot)$ denotes the trace of a (square) matrix.

2.3 Algorithm for MT-SGD

For the implementation of MT-SGD, we consider q as a discrete distribution over a set of M , ($M \in \mathbb{N}^*$) particles $\theta_1, \theta_2, \dots, \theta_M \sim q$. The formulation to evaluate U_{ij} in Equation. (3) becomes:

$$U_{ij} = \frac{1}{M^2} \sum_{a=1}^M \sum_{b=1}^M \left[k(\theta_a, \theta_b) \langle \nabla \log p_i(\theta_a), \nabla \log p_j(\theta_b) \rangle + \left\langle \nabla \log p_i(\theta_a), \frac{\partial k(\theta_a, \theta_b)}{\partial \theta_b} \right\rangle + \left\langle \nabla \log p_j(\theta_b), \frac{\partial k(\theta_a, \theta_b)}{\partial \theta_a} \right\rangle + \text{tr} \left(\frac{\partial^2 k(\theta_a, \theta_b)}{\partial \theta_a \partial \theta_b} \right) \right]. \quad (4)$$

The optimal solution ϕ_i^* then can be computed as:

$$\phi_i^*(\cdot) = \frac{1}{M} \sum_{j=1}^M [k(\theta_j, \cdot) \nabla_{\theta_j} \log p_i(\theta_j) + \nabla_{\theta_j} k(\theta_j, \cdot)]. \quad (5)$$

The key steps of our MT-SGD are summarized in Algorithm 1, where the set of particles $\theta_{1:M}$ is updated gradually to approach the multiple distributions $p_{1:K}$. Furthermore, the update formula consists of two terms: (i) the first term (i.e., relevant to $k(\theta_j, \cdot) \nabla_{\theta_j} \log p_i(\theta_j)$) helps to push the particles to the *joint high-likelihood region* for all distributions and (ii) the second term (i.e., relevant to $\nabla_{\theta_j} k(\theta_j, \cdot)$) which is a *repulsive term* to push away the particles when they reach out each other. Finally, we note that our proposed MT-SGD can be applied in the context where we know the target distributions up to a scaling factor (e.g., in the posterior inference).

¹All proofs and derivations can be found in the supplementary material.

Algorithm 1 Pseudocode for MT-SGD.

Input: Multiple unnormalized target densities $p_{1:K}$.

Output: The optimal particles $\theta_1, \theta_2, \dots, \theta_M$.

- 1: Initialize a set of particles $\theta_1, \theta_2, \dots, \theta_M \sim q_0$.
 - 2: **for** $t = 1$ to L **do**
 - 3: Form the matrix $U \in \mathbb{R}^{K \times K}$ with the element U_{ij} computed as in Equation. (4).
 - 4: Solve the QP $\min_{w \in \Delta_K} w^T U w$ to find the optimal weights $w^* \in \Delta_K$.
 - 5: Compute the optimal direction $\phi^*(\cdot) = \sum_{i=1}^K w_i^* \phi_i^*(\cdot)$, where ϕ_i^* is defined in Equation. (5).
 - 6: Update $\theta_i = \theta_i + \epsilon \phi^*(\theta_i), i = 1, \dots, K$.
 - 7: **end for**
 - 8: **return** $\theta_1, \theta_2, \dots, \theta_M$.
-

Analysis for the case of RBF kernel. We now consider a radial basis-function (RBF) kernel of bandwidth σ : $k(\theta, \theta') = \exp \left\{ -\|\theta - \theta'\|^2 / (2\sigma^2) \right\}$ and examine some asymptotic behaviors.

► **General case:** The elements of the matrix U become

$$U_{ij} = \mathbb{E}_{\theta, \theta' \sim q} \left[\exp \left\{ \frac{-\|\theta - \theta'\|^2}{2\sigma^2} \right\} \left[\langle \nabla \log p_i(\theta), \nabla \log p_j(\theta') \rangle + \frac{1}{\sigma^2} \langle \nabla \log p_i(\theta) - \nabla \log p_j(\theta'), \theta - \theta' \rangle - \frac{d}{\sigma^2} - \frac{\|\theta - \theta'\|^2}{\sigma^4} \right] \right].$$

► **Single particle distribution** $q = \delta_\theta$: The elements of the matrix U become

$$U_{ij} = \langle \nabla \log p_i(\theta), \nabla \log p_j(\theta) \rangle,$$

and our formulation reduces exactly to MOO in [8].

► **When** $\sigma \rightarrow \infty$: The elements of the matrix U become

$$U_{ij} = \mathbb{E}_{\theta, \theta' \sim q} \left[\langle \nabla \log p_i(\theta), \nabla \log p_j(\theta') \rangle \right].$$

2.4 Comparison to MOO-SVGD and Other Works

The most closely related work to ours is MOO-SVGD [17]. In a nutshell, ours is principally different from that work and we show a fundamental difference between our MT-SGD and MOO-SVGD in Figure 2. Our MT-SGD navigates the particles from one distribution to another distribution consecutively with a theoretical guarantee of globally getting closely to multiple target distributions. By contrast, while MOO-SVGD also uses the MOO [8] to update the particles, their employed repulsive term encourages the particle diversity without any theoretical-guaranteed principle to control the repulsive term, hence it can force the particles to scatter on the multiple distributions. In fact, they aim to profile the whole Pareto front, which is preferred when users want to obtain a collection of diverse Pareto optimal solutions with different trade-offs among all tasks.

Furthermore, it expects that our MT-SGD globally moves the set of particles to the *joint high-likelihood region* for all target distributions. Therefore, we do not claim our MT-SGD as a method to diversify the solution on a Pareto front for user preferences, as in [17, 19]. Alternatively, our MT-SGD

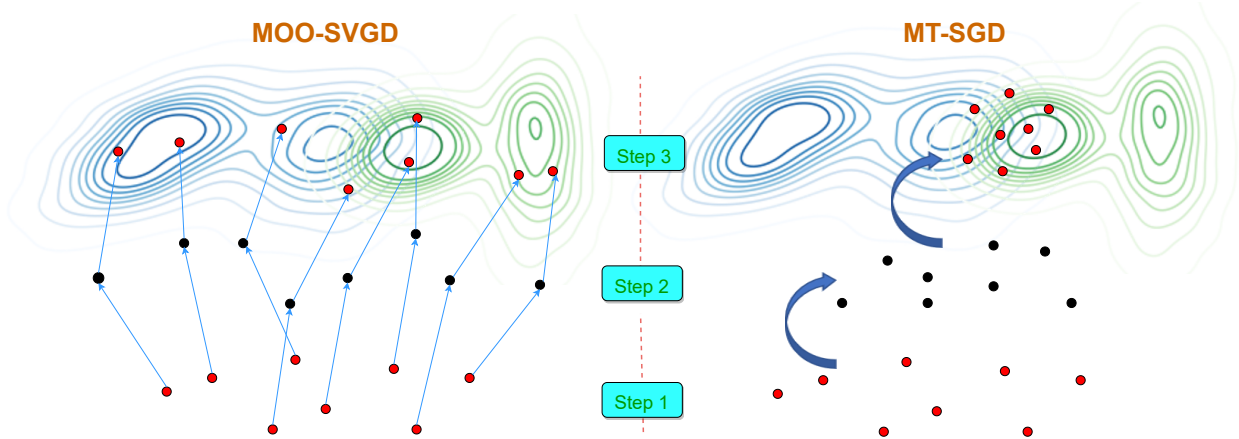


Figure 2: Our MT-SGD moves the particles from one distribution to another distribution to globally get closer to two target distributions (i.e., the blue and green ones). Differently, MOO-SVGD uses MOO [8] to move the particles individually and independently. The diversity is enforced by the repulsive forces among particles. There is no principle to control these repulsive forces, hence they can push the particles scattering on two distributions.

can generate diverse particles on the so-called *Pareto common* (i.e., the joint high-likelihood region for all target distributions). We argue and empirically demonstrate that by finding and diversifying the particles on Pareto common for the multiple posterior inferences, our MT-SGD can outperform the baselines on Bayesian-inference metrics such as the ensemble accuracy and the calibration error.

Moreover, MOO-SVGD is *not computationally efficient* when the number of particles is high because it requires solving an independent quadratic programming problem for each particle (cf. Section 4.1.1 and Figure 3 for the experiment on a synthetic dataset). Instead, our work solves a single quadratic programming problem for all particles, then update them accordingly. We verify this computational improvement and present the training time of all baselines in the supplement material.

3 Application to Multi-Task Learning

For multi-task learning, we assume to have K tasks $\{\mathcal{T}_i\}_{i=1}^K$ and a training set $\mathbb{D} = \{(x_i, y_{i1}, \dots, y_{iK})\}_{i=1}^N$, where x_i is a data example and y_{i1}, \dots, y_{iK} are the labels for the tasks. The model for each task $\theta^j = [\alpha, \beta^j]$, $j = 1, \dots, K$ consists of the *shared part* α and *non-shared part* β^j targeting the task j . The posterior $p(\theta^j | \mathbb{D})$ for each task reads

$$\begin{aligned} p(\theta^j | \mathbb{D}) &\propto p(\mathbb{D} | \theta^j) p(\theta^j) \propto \prod_{i=1}^N p(y_{ij} | x_i, \theta^j) \\ &\propto \prod_{i=1}^N \exp\{-\ell(y_{ij}, x_i; \theta^j)\} = \exp\left\{-\sum_{i=1}^N \ell(y_{ij}, x_i; \theta^j)\right\}, \end{aligned}$$

where ℓ is a loss function and the predictive likelihood $p(y_{ij} | x_i, \theta^j) \propto \exp\{-\ell(y_{ij}, x_i; \theta^j)\}$ is examined. Note that the prior $p(\theta^j)$ here is retained from previous studies [15, 17], which is a uniform and non-informative prior and can be treated as a constant term in our formulation.

Algorithm 2 Pseudocode for multi-task learning MT-SGD.

Input: A training set $\mathbb{D} = \{(x_i, y_{i1}, \dots, y_{iK})\}_{i=1}^N$.

Output: The models $\theta_m = [\theta_m^j]_{j=1}^K$ with $m = 1, \dots, M$, where $\theta_m^j = [\alpha_m, \beta_m^j]$.

```

1: Initialize a set of particles  $\theta_{1:M} \sim q_0$  .
2: for  $epoch = 1$  to  $\#epoch$  do
3:   for  $iter = 1$  to  $\#iter$  do
4:     Update the shared parts  $[\alpha_m]_{m=1}^M$  using Equation. (7).
5:     for  $j = 1$  to  $K$  do
6:       Update the non-shared part  $[\beta_m^j]_{m=1}^M$  using Equation. (9).
7:     end for
8:   end for
9: end for
10: return  $\theta_{1:M}$ .

```

For our approach, we maintain a set of models $\theta_m = [\theta_m^j]_{j=1}^K$ with $m = 1, \dots, M$, where $\theta_m^j = [\alpha_m, \beta_m^j]$. At each iteration, given the non-shared parts $[\beta^j]_{j=1}^K$ with $\beta^j = [\beta_m^j]_{m=1}^M$, we sample the shared parts from the multiple distributions $p(\alpha | \beta^j, \mathbb{D})$, $j = 1, \dots, K$ as

$$\alpha_m \sim p(\alpha | \beta^j, \mathbb{D}) \propto p(\alpha, \beta^j | \mathbb{D}) \propto p(\theta^j | \mathbb{D}) \propto \exp \left\{ - \sum_{i=1}^N \ell(y_{ij}, x_i; \theta^j) \right\}. \quad (6)$$

We now apply our proposed MT-SGD to sample the shared parts $[\alpha_m]_{m=1}^M$ from the multiple distributions defined in (6) as

$$\alpha_m = \alpha_m + \epsilon \sum_{j=1}^K w_j^* \phi_j^*(\alpha_m), \quad (7)$$

where $\phi_j^*(\alpha_m) = \frac{1}{M} \sum_{t=1}^M \left[k_1(\alpha_t, \alpha_m) \nabla_{\alpha_t} \log p(\alpha_t | \beta_t^j, \mathbb{D}) + \nabla_{\alpha_t} k_1(\alpha_t, \alpha_m) \right]$ and $w^* = [w_k^*]_{k=1}^K$ are the weights received from solving the quadratic programming problem. Here we note that $\nabla_{\alpha_t} \log p(\alpha_t | \beta_t^j, \mathbb{D})$ can be estimated via the batch gradient of the loss using Equation (6).

Given the updated shared parts $[\alpha_m]_{m=1}^M$, for each task j , we update the corresponding non-shared parts $[\beta_m^j]_{m=1}^M$ by sampling

$$\beta_m^j \sim p(\beta^j | \alpha, \mathbb{D}) \propto p(\beta^j, \alpha | \mathbb{D}) \propto p(\theta^j | \mathbb{D}) \propto \exp \left\{ - \sum_{i=1}^N \ell(y_{ij}, x_i; \theta^j) \right\}. \quad (8)$$

We now apply SVGD [16] to sample the non-shared parts $[\beta_m^j]_{m=1}^M$ for each task j from the distribution defined in (8) as

$$\beta_m^j = \beta_m^j + \epsilon \psi_j^*(\beta_m^j), \quad (9)$$

where $\psi_j^*(\beta_m^j) = \frac{1}{M} \sum_{a=1}^M \left[k_2(\beta_a^j, \beta_m^j) \nabla_{\beta_a^j} \log p(\beta_a^j | \alpha_a, \mathbb{D}) + \nabla_{\beta_a^j} k_2(\beta_a^j, \beta_m^j) \right]$ with which the term $\nabla_{\beta_a^j} \log p(\beta_a^j | \alpha_a, \mathbb{D})$ can be estimated via the batch loss gradient using Equation (8).

Algorithm 2 summarizes the key steps of our multi-task MT-SGD. Basically, we alternatively update the shared parts given the non-shared ones and vice versa.

4 Experiments

In this section, we verify our MT-SGD by evaluating its performance on both synthetic and real-world datasets. For our experiments, we use the RBF kernel $k(\theta, \theta') = \exp \left\{ -\|\theta - \theta'\|_2^2 / (2\sigma^2) \right\}$. The detailed training and configuration are given in the supplementary material. Our codes are available at <https://github.com/VietHoang1512/MT-SGD>.

4.1 Experiments on Toy Datasets

4.1.1 Sampling from Multiple Distributions

We first qualitatively analyze the behavior of the proposed method on sampling from three target distributions. Each target distribution is a mixture of two Gaussians as $p_i(\theta) = \pi_{i1}\mathcal{N}(\theta | \mu_{i1}, \Sigma_{i1}) + \pi_{i2}\mathcal{N}(\theta | \mu_{i2}, \Sigma_{i2})$ ($i = 1, 2, 3$) where the mixing proportions $\pi_{i1} = 0.7, \forall i$, $\pi_{i2} = 0.3, \forall i$, the means $\mu_{11} = [4, -4]^T$, $\mu_{12} = [0, 0.5]^T$, $\mu_{21} = [-4, 4]^T$, $\mu_{22} = [0.5, 0]^T$, and $\mu_{31} = [-3, -3]^T$, $\mu_{32} = [0, 0]^T$, and the common covariance matrix $\Sigma_{ij} = \begin{bmatrix} 0.5 & 0 \\ 0 & 0.5 \end{bmatrix}$, $i = 1, 2, 3$ and $j = 1, 2$. It can be seen from Figure 3 that there is a common high-density region spreading around the origin. The fifty particles are drawn randomly in the space, and the initialization is retained across experiments for a fair comparison.

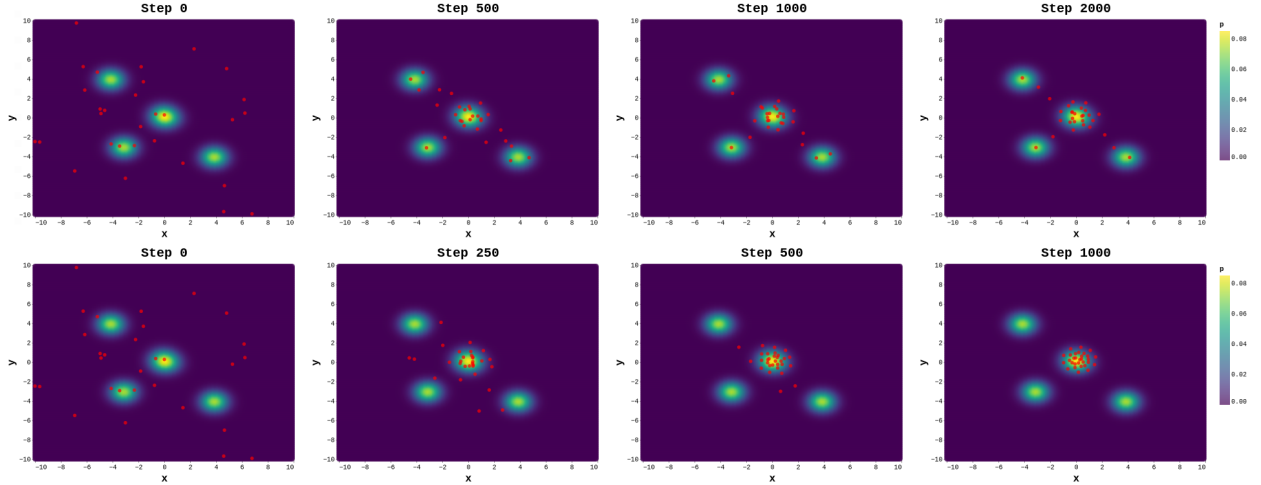


Figure 3: Sampling from three mixtures of two Gaussian distributions with a joint high-likelihood region. We run MOO-SVGd (top) and MT-SGD (bottom) to update the initialized particles (left-most figures) until convergence using Adam optimizer [13]. While MOO-SVGd transports the initialized particles scattering on the distributions, MT-SGD perfectly drives them to diversify in the region of interest.

Figure 3 shows the updated particles by MOO-SVGD and MT-SGD at selected iterations, we observe that the particles from MOO-SVGD spread out and tend to characterize all the modes, some of them even scattered along trajectories due to the conflict in optimizing multiple objectives. By contrast, our method is able to find and cover the common high density region among target distributions with well-distributed particles, which illustrates the basic principles of MT-SGD. Additionally, at the 1,000-th step, the training time for ours is 0.23 min, whereas that for MOO-SVGD is 1.63 min. The reason is that MOO-SVGD requires solving an independent quadratic programming problem for each particle at each step.

4.1.2 Multi-objective Optimization

The previous experiment illustrates that MT-SGD can be used to sample from multiple target distributions, we next test our method on the other low-dimensional multi-objectives OP from [33]. In particular, we use the two objectives ZDT3, whose Pareto front consists of non-contiguous convex parts, to show our method simultaneously minimizes both objective functions. Graphically, the simulation results from Figure 4 show the difference in the convergence behaviors between MOO-SVGD and MT-SGD: the solution set achieved by MOO-SVGD covers the entire Pareto front, while ours distributes and diversifies on the three middle curves (mostly concentrated in the middle curve) which are the Pareto common having low values for two objective functions in ZDT3.

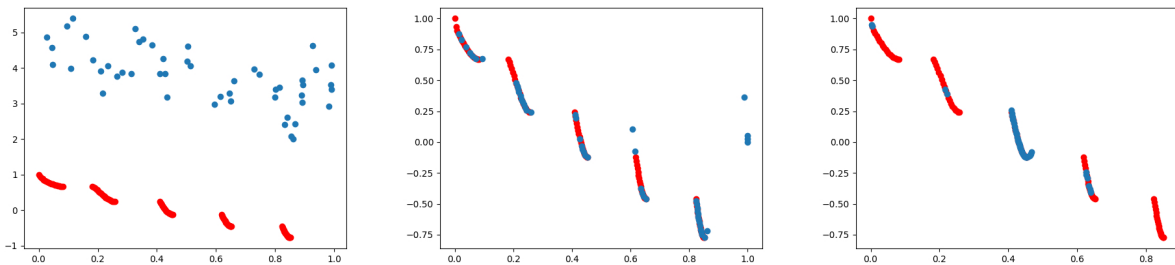


Figure 4: Solutions obtained by MOO-SVGD (mid) and MT-SGD (right) on ZDT3 problem after 10,000 steps, with blue points representing particles and red curves indicating the Pareto front. As expected, from initialized particles (left), MOO-SVGD’s solution set widely distributes on the whole Pareto front while the one of MT-SGD concentrates around middle curves (mostly the middle one).

4.2 Experiments on Real Datasets

4.2.1 Experiments on Multi-Fashion+Multi-MNIST Datasets

We apply the proposed MT-SGD method on multi-task learning, following Algorithm 2. Our method is validated on different benchmark datasets: (i) Multi-Fashion+MNIST [26], (ii) Multi-MNIST, and (iii) Multi-Fashion. Each of them consists of 120,000 training and 20,000 testing images generated from MNIST [14] and FashionMNIST [31] by overlaying an image on top of another: one in the top-left corner and one in the bottom-right corner. Lenet [14] (22,350 params) is employed as the backbone architecture and trained for 100 epochs with SGD in this experimental setup.

Baselines: In multi-task experiments, the introduced MT-SGD is compared with state-of-the-art baselines including MGDA [27], Pareto MTL [15], MOO-SVGD [17]. We note that to reproduce

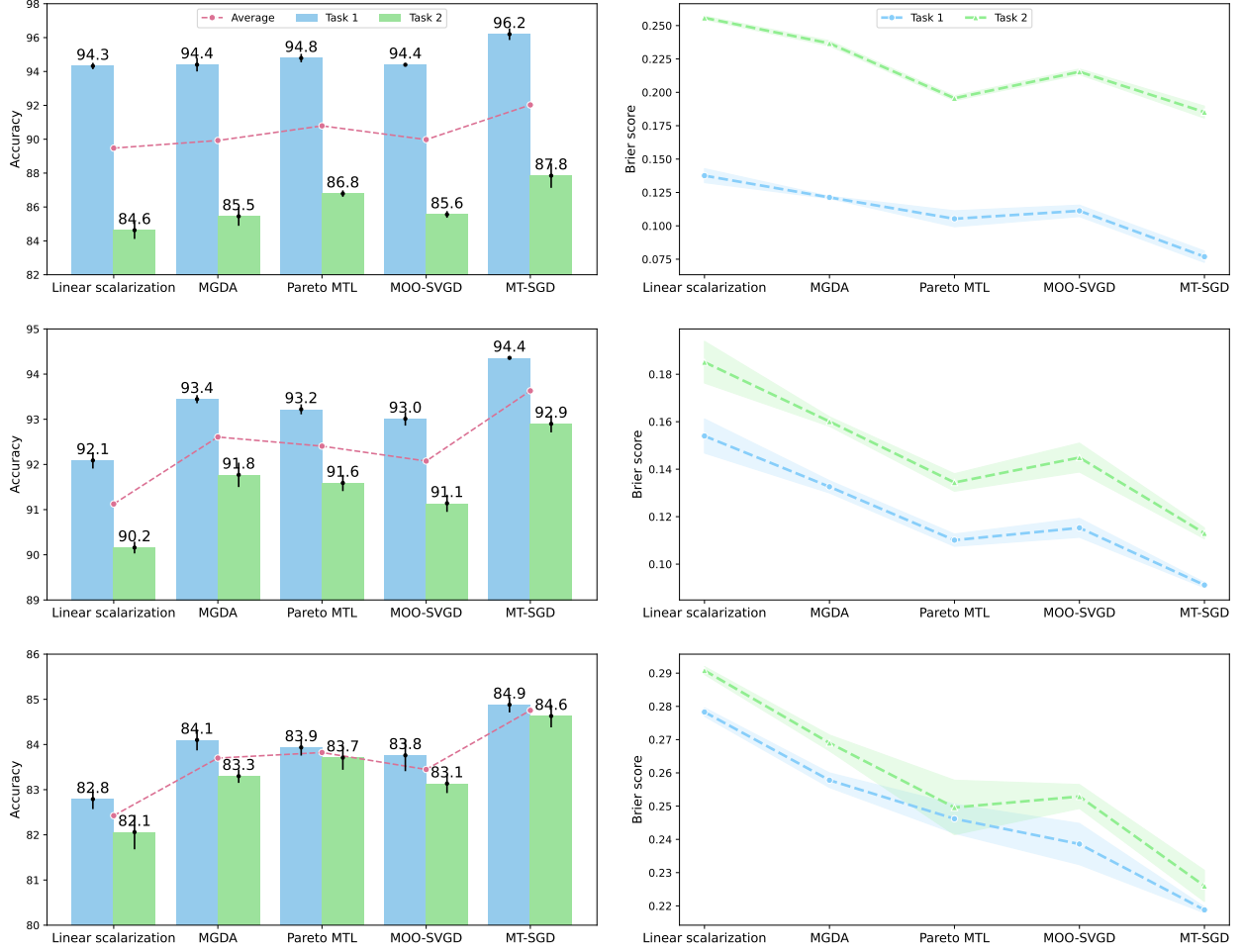


Figure 5: Results on Multi-Fashion+MNIST (left), Multi-MNIST (mid), and Multi-Fashion (right). We report the ensemble accuracy (*higher is better*) and the Brier score (*lower is better*) over 3 independent runs, as well as the standard deviation (the error bars and shaded areas in the figures).

results for these baselines, we either use the author’s official implementation released on GitHub or ask the authors for their codes. For MOO-SVGD and Pareto MTL, the reported result is from the ensemble prediction of five particle models. Additionally, for linear scalarization and MGDA, we train five particle models independently with different initializations and then ensemble these models.

Evaluation metrics: We compare MT-SGD against baselines regarding both average accuracy and predictive uncertainty. Besides the commonly used accuracy metric, we measure the quality and diversity of the particle models by relying on two other popular Bayesian metrics: Brier score [3, 23] and expected calibration error (ECE) [7, 21].

From Figure 5, we observe that MT-SGD consistently improves model performance across all tasks in both accuracy and Brier score by large margins, compared to existing techniques in the literature. The network trained using linear scalarization, as expected, produces inferior ensemble results while utilizing MOO techniques helps yield better performances. Overall, our proposed

method surpasses the second-best baseline by at least 1% accuracy in any experiment. Furthermore, Table 1 provides a comparison between these methods in terms of expected calibration error, in which MT-SGD also consistently provides the lowest expected calibration error, illustrating our method’s ability to obtain well-calibrated models (the accuracy is closely approximated by the produced confidence score). It is also worth noting that while Pareto MTL has higher accuracy, MOO-SVGD produces slightly better calibration estimation.

Table 1: Expected calibration error (%) (num_bin = 10) on Multi-MNIST, Multi-Fashion and Multi-Fashion+MNIST datasets over 3 runs. We use the **bold** font to highlight the best results

Dataset	Task	Linear scalarization	MGDA	Pareto MTL	MOO-SVGD	MT-SGD
Multi-Fashion+MNIST	Top left	21.33 \pm 0.83	19.91 \pm 0.26	9.44 \pm 0.65	9.47 \pm 0.89	4.65 \pm 0.11
	Bottom right	17.76 \pm 0.60	16.29 \pm 1.35	4.73 \pm 0.46	4.95 \pm 0.49	3.17 \pm 0.20
Multi-MNIST	Top left	17.37 \pm 0.62	15.29 \pm 0.49	5.45 \pm 0.85	5.37 \pm 0.51	3.28 \pm 0.20
	Bottom right	18.09 \pm 1.11	16.87 \pm 0.67	7.34 \pm 1.08	6.74 \pm 0.50	4.00 \pm 0.19
Multi-Fashion	Top left	15.86 \pm 1.20	14.48 \pm 0.95	8.55 \pm 0.69	5.48 \pm 0.53	3.80 \pm 0.38
	Bottom right	15.98 \pm 1.32	14.70 \pm 1.63	9.01 \pm 1.77	6.11 \pm 0.54	4.47 \pm 0.21

4.2.2 Experiment on CelebA Dataset

In this experiment, we verify the significance of MT-SGD on a larger neural network: Resnet18 [11], which consists of 11.4M parameters. We take the first 10 binary classification tasks and randomly select a subset of 40k images from the CelebA dataset [18]. Note that in this experiment, we consider Single task, in which 10 models are trained separately and serves as a strong baseline.

Table 2: Results on CelebA dataset, regarding accuracy and expected calibration error. For the full names of the tasks, please refer to our supplementary material. While MGDA trains a single model only to adapt on all tasks, reported performance of MOO-SVGD and MT-SGD is the ensemble results from five particle models.

	Method	5S	AE	Att	BUE	Bald	Bangs	BL	BN	BlaH	BloH	Average
Acc (%)	Single task	91.8	84.6	80.3	81.9	98.8	94.8	85.8	81.3	89.6	94.2	88.3
	MGDA	91.8	84.0	79.0	81.3	98.6	94.6	83.6	81.6	89.8	93.8	87.8
	MOO-SVGD	92.3	84.2	78.9	81.2	98.9	94.5	86.4	80.0	90.8	94.8	88.2
	MT-SGD	92.6	84.8	80.3	82.9	99.1	95.2	86.3	82.6	91.1	95.0	89.0
ECE (%)	Single task	3.3	2.4	4.4	3.9	0.7	1.6	5.7	6.5	3.1	1.1	3.3
	MGDA	1.4	1.1	3.5	7.3	0.3	1.8	6.9	5.4	2.1	1.2	3.1
	MOO-SVGD	2.8	1.9	3.1	5.6	0.3	0.5	4.7	3.3	1.3	1.3	2.5
	MT-SGD	1.2	1.4	1.7	2.3	0.6	1.7	6.8	1.2	2.1	0.9	2.0

The performance comparison of the mentioned models in CelebA experiment is shown in Table 2. As clearly seen from the upper part of the table, MT-SGD performs best in all tasks, except in BL, where MOO-SVGD is slightly better (86.4% vs 86.3%). Moreover, our method matches or beats Single task - the second-best baseline in all tasks. Regarding the well-calibrated uncertainty estimates, ensemble learning methods exhibit better results. In particular, MT-SGD and MOO-SVGD provide

the best calibration performances, which are 2% and 2.5%, respectively, which emphasizes the importance of efficient ensemble learning for enhanced calibration.

5 Conclusion

In this paper, we propose Stochastic Multiple Target Sampling Gradient Descent (MT-SGD), allowing us to sample the particles from the joint high-likelihood of multiple target distributions. Our MT-SGD is theoretically guaranteed to simultaneously reduce the divergences to the target distributions. Interestingly, the asymptotic analysis of our MT-SGD reduces exactly to the multi-objective optimization. We conduct comprehensive experiments to demonstrate that by driving the particles to the Pareto common (the joint high-likelihood of multiple target distributions), our MT-SGD can outperform the baselines on the ensemble accuracy and the well-known Bayesian metrics such as the expected calibration error and the Brier score.

Supplement to “Stochastic Multiple Target Sampling Gradient Descent”

These appendices provide supplementary details and results of MT-SGD, including our theory development and additional experiments. This consists of the following sections:

- Appendix A contains the proofs and derivations of our theory development.
- Appendix B contains the network architectures, experiment settings of our experiments and additional ablation studies.

A Proofs of Our Theory Development

A.1 Derivations for the Taylor expansion formulation

We have

$$\nabla_{\epsilon} D_{KL} \left(q^{[T]} \| p_i \right) \Big|_{\epsilon=0} = - \langle \phi, \psi_i \rangle_{\mathcal{H}_k^d}. \quad (10)$$

Proof of Equation (10): Since T is assumed to be an invertible mapping, we have the following equations:

$$D_{KL} \left(q^{[T]} \| p_i \right) = D_{KL} (T \# q \| p_i) = D_{KL} (q \| T^{-1} \# p_i)$$

and

$$D_{KL} (q \| T^{-1} \# p_i) = D_{KL} (q \| T^{-1} \# p_i) \Big|_{\epsilon=0} + \epsilon \nabla_{\epsilon} D_{KL} (q \| T^{-1} \# p_i) \Big|_{\epsilon=0} + O(\epsilon^2). \quad (11)$$

According to the change of variables formula, we have $T^{-1} \# p_i(\theta) = p_i(T(\theta)) |\det \nabla_{\theta} T(\theta)|$, then:

$$D_{KL} (q \| T^{-1} \# p_i) = \mathbb{E}_{\theta \sim q} [\log q(\theta) - \log p_i(T(\theta)) - \log |\det \nabla_{\theta} T(\theta)|].$$

Using this, the first term in Equation (11) is rewritten as:

$$\begin{aligned} D_{KL} (q \| p_i) &= D_{KL} (T \# q \| p_i) \Big|_{\epsilon=0} = D_{KL} (q \| T^{-1} \# p_i) \Big|_{\epsilon=0} \\ &= \mathbb{E}_{\theta \sim q} [\log q(\theta) - \log p_i(\theta) - \log |\det \nabla_{\theta} \theta|] = \mathbb{E}_{\theta \sim q} [\log q(\theta) - \log p_i(\theta)]. \end{aligned} \quad (12)$$

Similarly, the second term in Equation (11) could be expressed as:

$$\begin{aligned} \nabla_{\epsilon} D_{KL} (q \| T^{-1} \# p_k) \Big|_{\epsilon=0} &= \mathbb{E}_{\theta \sim q} [\nabla_{\epsilon} \log q(\theta) - \nabla_{\epsilon} \log p_i(T(\theta)) - \nabla_{\epsilon} \log |\det \nabla_{\theta} T(\theta)|] \Big|_{\epsilon=0} \\ &= -\mathbb{E}_{\theta \sim q} [\nabla_{\epsilon} \log p_i(T(\theta)) + \nabla_{\epsilon} \log |\det \nabla_{\theta} T(\theta)|] \Big|_{\epsilon=0} \\ &= -\mathbb{E}_{\theta \sim q} [\nabla_T \log p_i(T(\theta)) \nabla_{\epsilon} T(\theta)] \Big|_{\epsilon=0} \\ &\quad - \mathbb{E}_{\theta \sim q} \left[\frac{1}{|\det \nabla_{\theta} T(\theta)|} \frac{|\det \nabla_{\theta} T(\theta)|}{\det \nabla_{\theta} T(\theta)} \nabla_{\epsilon} \det \nabla_{\theta} T(\theta) \right] \Big|_{\epsilon=0} \quad (13) \\ &= -\mathbb{E}_{\theta \sim q} [\nabla_T \log p_i(T(\theta)) \phi(\theta)] \Big|_{\epsilon=0} \\ &\quad - \mathbb{E}_{\theta \sim q} p \left[\frac{\det \nabla_{\theta} T(\theta) \operatorname{tr}((\nabla_{\theta} T(\theta))^{-1} \nabla_{\epsilon} \nabla_{\theta} T(\theta))}{\det \nabla_{\theta} T(\theta)} \right] \Big|_{\epsilon=0} \\ &= -\mathbb{E}_{\theta \sim q} [\nabla_{\theta} \log p_i(\theta) \phi(\theta) + \operatorname{tr}(\nabla_{\theta} \phi(\theta))]. \end{aligned}$$

It could be shown from the reproducing property of the RKHS that $\phi_i(\theta) = \langle \phi_i(\cdot), k(\theta, \cdot) \rangle_{\mathcal{H}_k}$, then we find that

$$\frac{\partial \phi_i(\theta)}{\partial \hat{\theta}_i} = \left\langle \phi_i(\cdot), \frac{\partial k(\theta, \cdot)}{\partial \hat{\theta}_i} \right\rangle_{\mathcal{H}_k}. \quad (14)$$

Let $U_{d \times d} = \nabla_{\theta} \phi(\theta)$ whose u_i^T denotes the i^{th} row vector and the particle $\theta \in \mathbb{R}^d$ is represented by $\{\hat{\theta}\}_{i=1}^d$, the row vector u_i^T is given by:

$$u_i^T := \frac{\partial \phi_i(\theta)}{\partial \theta} = \frac{\partial \phi_i(\theta)}{\partial (\hat{\theta}_1, \hat{\theta}_2, \dots, \hat{\theta}_d)} = \left[\frac{\partial \phi_i(\theta)}{\partial \hat{\theta}_1}, \frac{\partial \phi_i(\theta)}{\partial \hat{\theta}_2}, \dots, \frac{\partial \phi_i(\theta)}{\partial \hat{\theta}_d} \right]. \quad (15)$$

Combining Property (14) and Equation (15), we have:

$$\begin{aligned} u_i^T &:= \left[\frac{\partial \phi_i(\theta)}{\partial \hat{\theta}_1}, \frac{\partial \phi_i(\theta)}{\partial \hat{\theta}_2}, \dots, \frac{\partial \phi_i(\theta)}{\partial \hat{\theta}_d} \right] \\ &= \left[\left\langle \phi_i(\cdot), \frac{\partial k(\theta, \cdot)}{\partial \hat{\theta}_1} \right\rangle_{\mathcal{H}_k}; \left\langle \phi_i(\cdot), \frac{\partial k(\theta, \cdot)}{\partial \hat{\theta}_2} \right\rangle_{\mathcal{H}_k}; \dots; \left\langle \phi_i(\cdot), \frac{\partial k(\theta, \cdot)}{\partial \hat{\theta}_d} \right\rangle_{\mathcal{H}_k} \right]. \end{aligned} \quad (16)$$

Substituting Equation (16) to Equation (13), the linear term of the Taylor expansion could be derived as:

$$\begin{aligned} \nabla_{\epsilon} D_{KL}(q || T^{-1} \# p_i) \big|_{\epsilon=0} &= -\mathbb{E}_{\theta \sim q} [\nabla_{\theta} \log p_i(\theta) \phi(\theta) + \text{tr}(\nabla_{\theta} \phi(\theta))] \\ &= -\mathbb{E}_{\theta \sim q} \left[\sum_{j=1}^d \langle \phi_j(\cdot), k(\theta, \cdot) \rangle_{\mathcal{H}_k} (\nabla_{\theta} \log p_i(\theta))_j + \frac{\partial \phi_j(\theta)}{\partial \hat{\theta}_j} \right] \\ &= -\sum_{j=1}^d \mathbb{E}_{\theta \sim q} \left[\langle \phi_j(\cdot), k(\theta, \cdot) (\nabla_{\theta} \log p_i(\theta))_j \rangle_{\mathcal{H}_k} + \left\langle \phi_j(\cdot), \left(\frac{\partial k(\theta, \cdot)}{\partial \theta} \right)_j \right\rangle_{\mathcal{H}_k} \right] \\ &= -\sum_{j=1}^d \left\langle \phi_j(\cdot), \mathbb{E}_{\theta \sim q} \left[k(\theta, \cdot) (\nabla_{\theta} \log p_i(\theta))_j + \left(\frac{\partial k(\theta, \cdot)}{\partial \theta} \right)_j \right] \right\rangle_{\mathcal{H}_k} \\ &= -\langle \phi(\cdot), \psi(\cdot) \rangle_{\mathcal{H}_k^d}, \end{aligned}$$

where $(v)_j$ denotes the j -th element of v and $\psi(\cdot) \in \mathcal{H}_k^d$ is a matrix whose j^{th} column vector is given by

$$\mathbb{E}_{\theta \sim q} \left[k(\theta, \cdot) (\nabla_{\theta} \log p_i(\theta))_j + \left(\frac{\partial k(\theta, \cdot)}{\partial \theta} \right)_j \right].$$

In other word, the formula of $\psi(\cdot)$ becomes

$$\mathbb{E}_{\theta \sim q} \left[k(\theta, \cdot) \nabla_{\theta} \log p_i(\theta) + \frac{\partial k(\theta, \cdot)}{\partial \theta} \right].$$

As a consequence, we obtain the conclusion of Equation (10).

A.2 Proof of Lemma 1

Before proving this lemma, let us re-state it:

Lemma 3. Let w^* be the optimal solution of the optimization problem $w^* = \underset{w \in \Delta_K}{\operatorname{argmin}} w^T U w$ and $\phi^* = \sum_{i=1}^K w_i^* \phi_i^*$, where $\Delta_K = \{\pi \in \mathbb{R}_+^K : \|\pi\|_1 = 1\}$ and $U \in \mathbb{R}^{K \times K}$ with $U_{ij} = \left\langle \phi_i^*, \phi_j^* \right\rangle_{\mathcal{H}_k^d}$, then we have

$$\langle \phi^*, \phi_i^* \rangle_{\mathcal{H}_k^d} \geq \|\phi^*\|_{\mathcal{H}_k^d}^2, i = 1, \dots, K.$$

Proof. For arbitrary $\epsilon \in [0, 1]$ and $u \in \Delta_K$, then $\omega := \epsilon u + (1 - \epsilon)w^* \in \Delta_K$, we thus have the following inequality:

$$\begin{aligned} w^{*T} U w^* &\leq \omega^T U \omega \\ &= (\epsilon u + (1 - \epsilon)w^*)^T U (\epsilon u + (1 - \epsilon)w^*) \\ &= (w^* + \epsilon(u - w^*))^T U (w^* + \epsilon(u - w^*)) \\ &= w^{*T} U w^* + 2\epsilon w^{*T} U (u - w^*) + \epsilon^2 (u - w^*)^T U (u - w^*), \end{aligned}$$

which is equivalent to

$$0 \leq 2\epsilon w^{*T} U (u - w^*) + \epsilon^2 (u - w^*)^T U (u - w^*). \quad (17)$$

Hence $w^{*T} U (u - w^*) \geq 0$, since otherwise the R.H.S of inequality (17) will be negative with sufficiently small ϵ . By that, we arrive at

$$w^{*T} U w^* \leq w^{*T} U u.$$

By choosing u to be a one hot vector at i , we obtain the conclusion of Lemma 1.

A.3 Derivations for the matrix U_{ij} 's formulation in Equation (3)

We have

$$\begin{aligned} \phi_i^* (\cdot) &= \mathbb{E}_{\theta \sim q} [k(\theta, \cdot) \nabla \log p_i(\theta) + \nabla k(\theta, \cdot)], \\ \phi_j^* (\cdot) &= \mathbb{E}_{\theta' \sim q} [k(\theta', \cdot) \nabla \log p_j(\theta') + \nabla k(\theta', \cdot)]. \end{aligned}$$

Therefore, we find that

$$\begin{aligned} U_{ij} = \langle \phi_i^*, \phi_j^* \rangle_{\mathcal{H}_k^d} &= \mathbb{E}_{\theta, \theta' \sim q} \left[\langle k(\theta, \cdot), k(\theta', \cdot) \rangle_{\mathcal{H}_k} \sum_{l=1}^d \nabla_{\theta_l} \log p_i(\theta) \nabla_{\theta'_l} \log p_j(\theta') \right. \\ &\quad + \sum_{l=1}^d \nabla_{\theta_l} \log p_i(\theta) \langle k(\theta, \cdot), \nabla_{\theta'_l} k(\theta', \cdot) \rangle_{\mathcal{H}_k} + \sum_{l=1}^d \nabla_{\theta'_l} \log p_j(\theta') \langle k(\theta', \cdot), \nabla_{\theta_l} k(\theta, \cdot) \rangle_{\mathcal{H}_k} \\ &\quad \left. + \sum_{l=1}^d \langle \nabla_{\theta_l} k(\theta, \cdot), \nabla_{\theta'_l} k(\theta', \cdot) \rangle_{\mathcal{H}_k} \right], \end{aligned}$$

which is equivalent to

$$\begin{aligned}
U_{ij} = \mathbb{E}_{\theta, \theta' \sim q} & \left[k(\theta, \theta') \langle \nabla \log p_i(\theta), \nabla \log p_j(\theta') \rangle \right. \\
& + \left\langle \nabla \log p_i(\theta), \frac{\partial k(\theta, \theta')}{\partial \theta'} \right\rangle + \left\langle \nabla \log p_j(\theta'), \frac{\partial k(\theta, \theta')}{\partial \theta} \right\rangle + \\
& \left. + \sum_{l=1}^d \left\langle \nabla_{\theta_l} k(\theta, \cdot), \nabla_{\theta'_l} k(\theta', \cdot) \right\rangle_{\mathcal{H}_k} \right].
\end{aligned}$$

Now, note that

$$\langle k(\theta, \cdot), \varphi(\cdot) \rangle_{\mathcal{H}_k} = \varphi(\theta),$$

hence we gain

$$\langle \nabla_{\theta_l} k(\theta, \cdot), \varphi(\cdot) \rangle_{\mathcal{H}_k} = \nabla_{\theta_l} \varphi(\theta),$$

which follows that

$$\begin{aligned}
& \left\langle \nabla_{\theta_l} k(\theta, \cdot), \nabla_{\theta'_l} k(\theta', \cdot) \right\rangle_{\mathcal{H}_k} = \nabla_{\theta_l, \theta'_l}^2 k(\theta, \theta'), \\
& \sum_{l=1}^d \left\langle \nabla_{\theta_l} k(\theta, \cdot), \nabla_{\theta'_l} k(\theta', \cdot) \right\rangle_{\mathcal{H}_k} = \sum_{l=1}^d \nabla_{\theta_l, \theta'_l}^2 k(\theta, \theta') = \text{tr} \left(\frac{\partial^2 k(\theta, \theta')}{\partial \theta \partial \theta'} \right).
\end{aligned}$$

Putting these results together, we obtain that

$$\begin{aligned}
U_{ij} = \langle \phi_i^*, \phi_j^* \rangle_{\mathcal{H}_k^d} = \mathbb{E}_{\theta, \theta' \sim q} & \left[k(\theta, \theta') \langle \nabla \log p_i(\theta), \nabla \log p_j(\theta') \rangle \right. \\
& + \left\langle \nabla \log p_i(\theta), \frac{\partial k(\theta, \theta')}{\partial \theta'} \right\rangle + \left\langle \nabla \log p_j(\theta'), \frac{\partial k(\theta, \theta')}{\partial \theta} \right\rangle + \text{tr} \left(\frac{\partial^2 k(\theta, \theta')}{\partial \theta \partial \theta'} \right) \Big].
\end{aligned}$$

As a consequence, we obtain the conclusion of Equation (3).

A.4 Proof of Theorem 2

Before proving this theorem, let us re-state it:

Theorem 4. *w ∈ Δ_K such that ∑_{i=1}^K w_iϕ_i^{*} = 0, given a sufficiently small step size ε, all KL divergences w.r.t. the target distributions are strictly decreased by at least A ‖ϕ^{*}‖_{ℋ_k^d}² > 0 where A is a positive constant.*

Proof. We have for all i = 1, ..., K that

$$\begin{aligned}
D_{KL} \left(q^{[T]} \| p_i \right) &= D_{KL} (q \| p_i) + \nabla_{\epsilon} D_{KL} \left(q^{[T]} \| p_i \right) \Big|_{\epsilon=0} \epsilon + O_i(\epsilon^2) \\
&= D_{KL} (q \| p_i) - \langle \phi, \psi_i \rangle_{\mathcal{H}_k^d} \epsilon + O_i(\epsilon^2) \\
&\leq D_{KL} (q \| p_i) - \|\phi^*\|_{\mathcal{H}_k^d}^2 \epsilon + O_i(\epsilon^2).
\end{aligned}$$

Because $\lim_{\epsilon \rightarrow 0} \frac{O_i(\epsilon^2)}{\epsilon^2} = B_i$, there exists $\alpha_i > 0$ such that $|\epsilon| < \alpha_i$ implies $|O_i(\epsilon^2)| < \frac{3}{2} |B_i| \epsilon^2$. By choosing, $B = \frac{3}{2} \max_i |B_i|$ and $\alpha = \min_i \alpha_i$, we arrive at for all $\epsilon < \alpha$ and all i

$$D_{KL} \left(q^{[T]} \| p_i \right) < D_{KL} (q \| p_i) - \|\phi^*\|_{\mathcal{H}_k^d}^2 \epsilon + B \epsilon^2.$$

Finally, by choosing sufficiently small $\epsilon > 0$, we reach the conclusion of the theorem. \square

B Implementation Details

In this appendix, we provide implementation details regarding the empirical evaluation in the main paper along with additional comparison experiments.

B.1 Experiments on Toy Datasets

B.1.1 Sampling from Multiple Distribution

In this experiment, the three target distributions are created as presented in the main paper. The particle’s coordinates are randomly sampled from the normal distribution $\mathcal{N}(0, 5)$. Adam optimizer [13] with learning rate of $3e-2$ and $\beta_1 = 0.9, \beta_2 = 0.999$ is used to update the particles. MOO-SVGD and MT-SGD converged after 2000 and 1000 iterations, respectively.

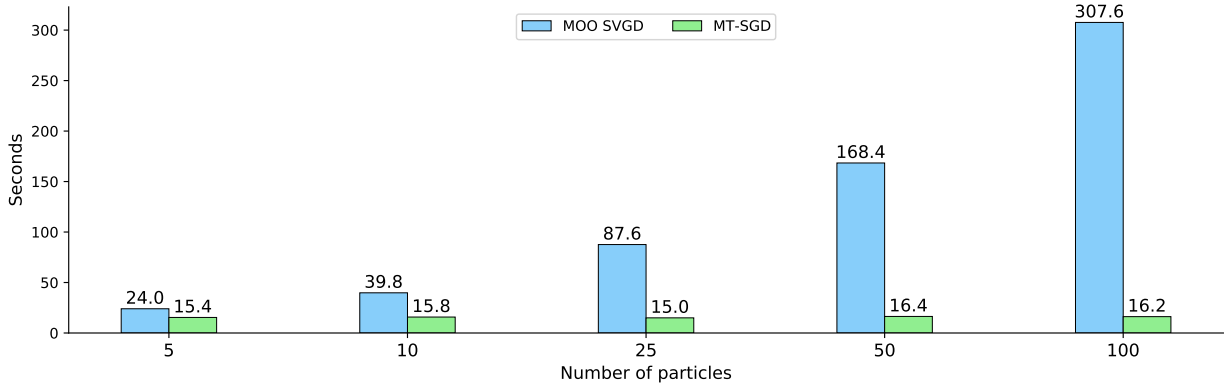


Figure 6: Running time of MT-SGD and MOO-SVGD for 1000 steps on: Intel(R) Xeon(R) CPU @ 2.20GHz CPU and Tesla T4 16GB VRAM GPU. Results are averaged over 5 runs.

We also measure the running time between MOO-SVGD and our proposed method when varying the number of particles from 5 to 100. In Figure 6, we plot the time consumption when running MOO-SVGD and MT-SGD in 1000 iterations. As can be seen that, MOO-SVGD runtime grows linearly with the number of particles, since it requires solving separate quadratic problems (Algorithm 1) for each particle. By contrast, there is only one quadratic programming problem solving in our proposed method, which significantly reduces time complexity, especially when the number of particles is high.

B.1.2 Multi-objective Optimization

ZDT-3 [33] is a classic benchmark problem in multi-objective optimization with 30 variables $\theta = (\theta_1, \theta_2, \dots, \theta_{30})$ with a number of disconnected Pareto-optimal fronts. This problem is given by:

$$\begin{aligned} \min f_1(\theta), \\ \min f_2(\theta) = g(\theta)h(f_1(\theta), g(\theta)), \end{aligned}$$

where

$$\begin{aligned}
f_1(\theta) &= \theta_1, \\
g(\theta) &= 1 + \frac{9}{29} \sum_{i=2}^{30} \theta_i, \\
h(f_1, g) &= 1 - \sqrt{\frac{f_1}{g}} - \frac{f_1}{g} \sin(10\pi f_1), \\
0 \leq \theta_i &\leq 1, i = 1, 2, \dots, 30.
\end{aligned}$$

The Pareto optimal solutions are given by

$$\begin{aligned}
0 \leq \theta_1 &\leq 0.0830, \\
0.1822 \leq \theta_1 &\leq 0.257, \\
0.4093 \leq \theta_1 &\leq 0.4538, \\
0.6183 \leq \theta_1 &\leq 0.6525, \\
0.8233 \leq \theta_1 &\leq 0.8518, \\
\theta_i = 0 &\text{ for } i = 2, \dots, 30.
\end{aligned}$$

For ZDT3 experiment, we utilize Adam [13], learning rate $5e-4$ and update the 50 particles for 10000 iterations as in the comparative baseline [17].

B.1.3 Multivariate regression

We consider the SARCOS regression dataset [28], which contains 44,484 training samples and 4,449 testing samples with 21 input variables and 7 outputs (tasks). The train-test split in [22] is kept, with 40,036 training examples, 4,448 validation examples, and 4,449 test examples. We replicate the neural network architecture from [22] as follows: $21 \times 256 \text{ FC} \rightarrow \text{ReLU} \rightarrow 256 \times 256 \text{ FC} \rightarrow \text{ReLU} \rightarrow 256 \times 256 \text{ FC} \rightarrow \text{ReLU} \rightarrow 256 \times 7 \text{ FC}$ (139,015 params). The network is optimized by Adam [13] optimizer for 1000 epochs, with $\beta_1 = 0.9$, $\beta_2 = 0.999$, and the learning rate of $1e-4$. All experimental results are obtained by running five times with different seeds.

Table 3: Mean square errors of MT-SGD and competing methods on SARCOS dataset [28]. We take the best checkpoint in each approach based on the validation score. Results are averaged over 5 runs, and we highlight the best method for each task in **bold**.

	Method	Task 1	Task 2	Task 3	Task 4	Task 5	Task 6	Task 7	Average
Validation	MGDA	0.025	0.2789	0.0169	0.0026	1.158	0.264	0.005	0.25
	MOO-SVGD	0.0177	0.2182	0.0113	0.0013	1.241	0.2292	0.0025	0.2459
	MT-SGD	0.0173	0.2124	0.0112	0.0012	1.110	0.2208	0.0024	0.2251
Test	MGDA	0.0082	0.0675	0.0038	0.0009	0.2635	0.0455	0.0018	0.0559
	MOO-SVGD	0.0043	0.0586	0.0019	0.0003	0.2584	0.0365	0.0007	0.0515
	MT-SGD	0.0037	0.0515	0.0018	0.0002	0.2097	0.0318	0.0005	0.0428

Regarding the baselines for this experiment, we compare our method against MGDA [27], MOO-SVGD [17]. We empirically set the batch size as 512 and $M = 5$ particles in MT-SGD and competing

methods. The mean square error for each task and the average results are shown in Table 3. We find that our method achieves the lowest error on all tasks, with the largest gap on Task 4. MT-SGD outperforms the second-best method, MOO-SVGD, with 0.2251 vs. 0.2459 on validation set and 0.0428 vs. 0.0515 on test set.

B.2 Experiments on Real Datasets

B.2.1 Experiments on Multi-Fashion+Multi-MNIST Datasets

We follow the same training protocol with previous work [15, 17, 27], Lenet [14] is trained in 100 epochs with SGD optimizer. The input images are in size 36×36 and the training batch size is 256.

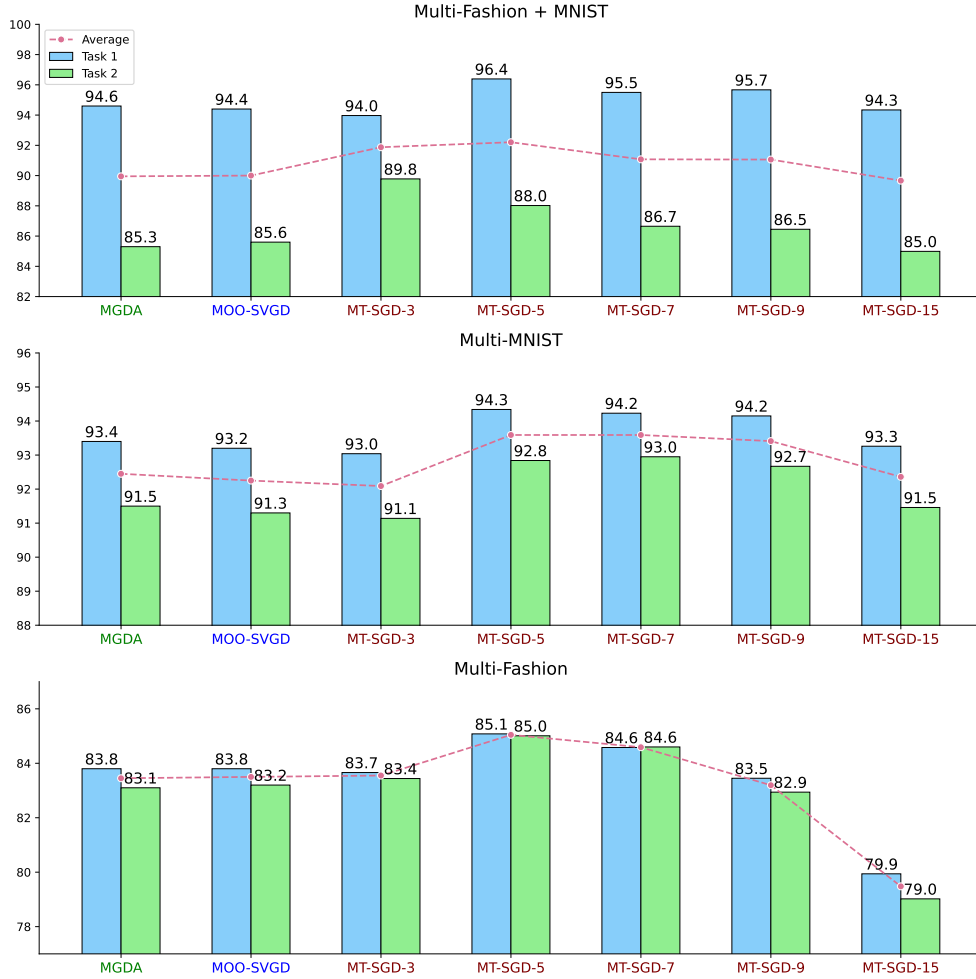


Figure 7: Average accuracy (%) when varying the number of particles from 3 to 15. **MT-SGD-m** denotes our method using m particle networks.

We now study the performance of our proposed method against variation in the number of particles by conducting more experiments on Multi-MNIST/Fashion/Fashion+MNIST datasets. We vary the number of neural networks in 3, 5, 7, 9, 15 and present the accuracy scores in Figure 7. From

the results, a simple conclusion that can be derived is that increasing the number of particle networks from $3 \rightarrow 5$ improves the performance in all three datasets, surpassing the other two baselines, while further increasing this hyperparameter does not help.

Metrics: In the main paper, we compare our proposed method against baselines in terms of Brier score and expected calibration error (ECE). We here provide more details on how to calculate these metrics. Assumed that the training dataset \mathcal{D} consists of N i.i.d examples $\mathcal{D} = \{x_n, y_n\}_{n=1}^N$ where $y_n \in \{1, 2, \dots, K\}$ denotes corresponding labels for K-class classification problem. Let $p(y = c|x_i)$ be the predicted confidence that x_i belongs to class C.

- **Brier score:** The Brier score is computed as the squared error between a predicted probability $p(y|x_i)$ and the one-hot vector ground truth:

$$BS = \frac{1}{N} \sum_{i=1}^N \sum_{c=1}^K \left(\mathbf{1}_{y_i=c} - p(y = c|x_i) \right)^2$$

- **Expected calibration error:** Partitioning predictions into M equally-spaced bins $B_m = \left(\frac{m-1}{M}, \frac{m}{M} \right] (m = 1, 2, \dots, M)$, the expected calibration error is computed as the average gap between the accuracy and the predicted confidence within each bin:

$$ECE = \sum_{m=1}^M \frac{|B_m|}{N} |\text{acc}(B_m) - \text{conf}(B_m)|$$

where $\text{acc}(B_m)$ and $\text{conf}(B_m)$ denote the accuracy and confidence of bin B_m

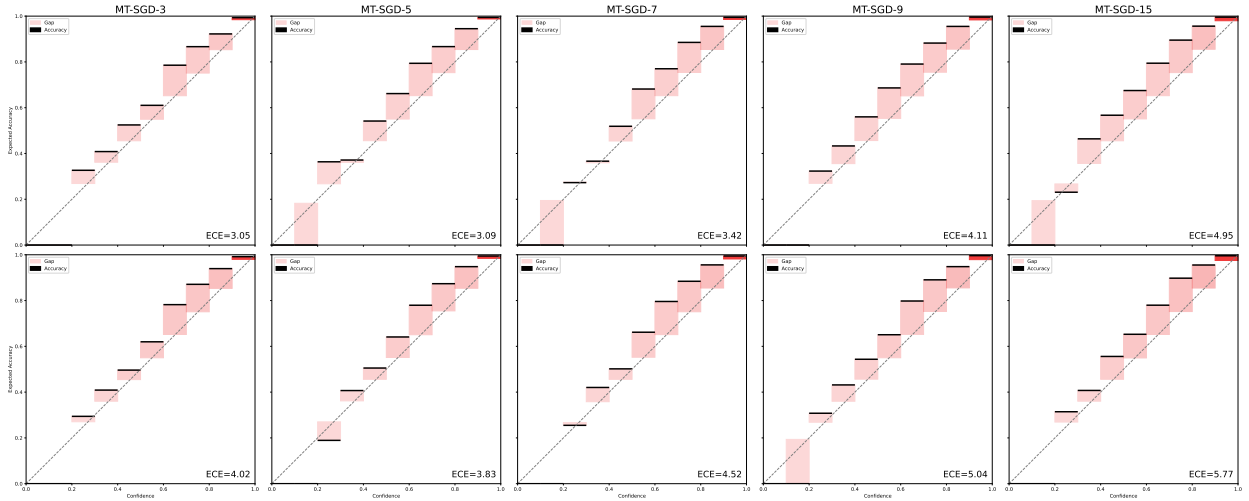


Figure 8: Expected Calibration Error (%) when varying the number of particles from 3 to 15 on Multi-MNIST. MT-SGD-m denotes our method using m particle networks. We set the number of bins equal to 10 throughout the experiments.

Figure 8 displays ECE as a function of the number of particles. Similar to the average accuracy metric, the Expected Calibration Error reduces when we increase the number of particle networks from 3 to 5 yet does not decrease in the cases of MT-SGD-7, MT-SGD-9 and MT-SGD-15.

Computational complexity of MT-SGD: From the complexity point of view, MT-SGD introduces a marginal computational overhead compared to MGDA since it requires calculating the matrix U , which has a complexity $O(K^2 M^2 d)$, where the number of particles M is usually set to a small positive integer. However, on the one hand, computing U 's entries can be accelerated in practice by calculating them in parallel since there is no interaction between them during forward pass. On the other hand, the computation of the back-propagation is typically more costly than the forward pass. Thus, the main bottlenecks in our method lie on the backward pass and solving the quadratic programming problem - which is an iterative method [?, 27].

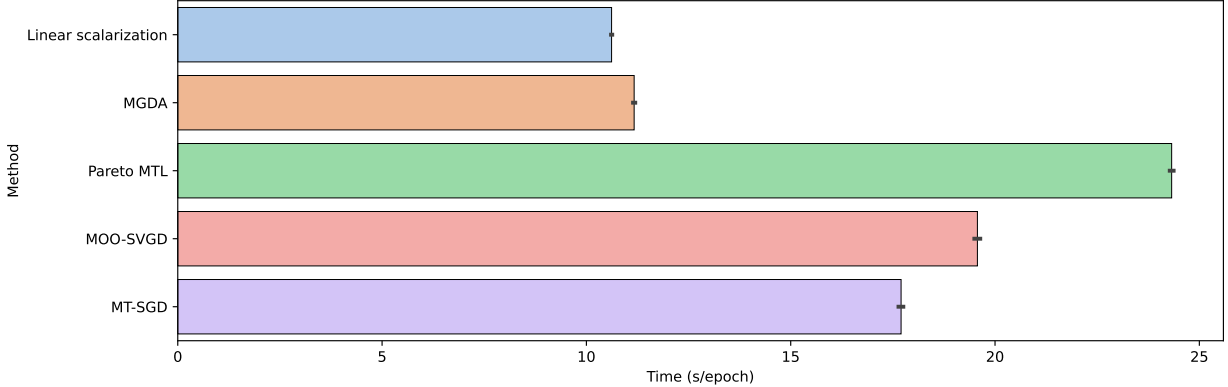


Figure 9: Running time on each epoch of MT-SGD and compared baselines on Multi-MNIST dataset. Results are averaged over 5 runs, with the standard deviation reported by error bars.

As a final remark in the Multi-Fashion+Multi-MNIST experiment, we compare our methods against baselines in terms of the required running time in a single epoch and plot the result in Figure 9. We observe that in our experiments on Multi-MNIST dataset, the computation time of methods that enforce the diversity of obtained models is higher than that of the methods that do not (Pareto MTL, MOO-SVGD, MT-SGD vs Linear scalarization, MGDA). Nevertheless, this is a small price to pay for the major gain in the ensemble performance, since our training involves the interaction between models to impose diversity. Compared to Pareto MTL and MOO-SVGD, the running time of our proposed MT-SGD is considerably better (2s less than MOO-SVGD and 6s less than Pareto MTL).

B.2.2 Experiment on CelebA Dataset

We performed our experiments on the CelebA dataset [18], which contains images annotated with 40 binary attributes. Resnet-18 backbone [11] without the final layer as a shared encoder and a 2048 x 2 dimensional fully connected layer for each task is employed as in [27]. We train this network for 100 epochs with Adam optimizer [13] of learning rate $5e - 4$ and batch size 64. All images are resized to $64 \times 64 \times 3$.

Due to space constraints, we report only the abbreviation of each task in the main paper, their full names are presented below.

Now we investigate the effectiveness of our proposed MT-SGD method on the whole CelebA dataset, compared with prior work: Uniform scaling: minimizing the uniformly weighted sum of objective functions, Single task: train separate models individually for each task, Uncertainty [12]:

Table 4: CelebA binary classification tasks full names.

5S	AE	Att	BUE	Bald	Bangs	BL	BN	BlaH	BloH
5 O'clock Shadow	Arched Eyebrows	Attractive	Bags Under Eyes	Bald	Bangs	Big Lips	Big Nose	Black Hair	Blond Hair

adaptive reweighting with balanced uncertainty, Gradnorm [4]: balance the loss functions via gradient magnitude and MGDA [27]. The results from previous work are reported in [4]. For MGDA, we use their officially released codebase at <https://github.com/isl-org/MultiObjectiveOptimization>. For a fair comparison, we run the code with five different random seeds and present the obtained scores in Figure 10.

Following [27], we divide 40 target binary attributes into two subgroups: hard and easy tasks for easier visualization. As can be seen from Figure 10, we observe that the naively trained Uniform scaling has relatively low performance on many tasks, e.g. “Mustache”, “Big Lips”, “Oval Face”. Compared to other baselines, our proposed method significantly reduces the prediction error in almost all the tasks, especially on “Goatee”, “Double Chi” and “No Beard”. The detailed result for each target attribute can be found in Table 5.

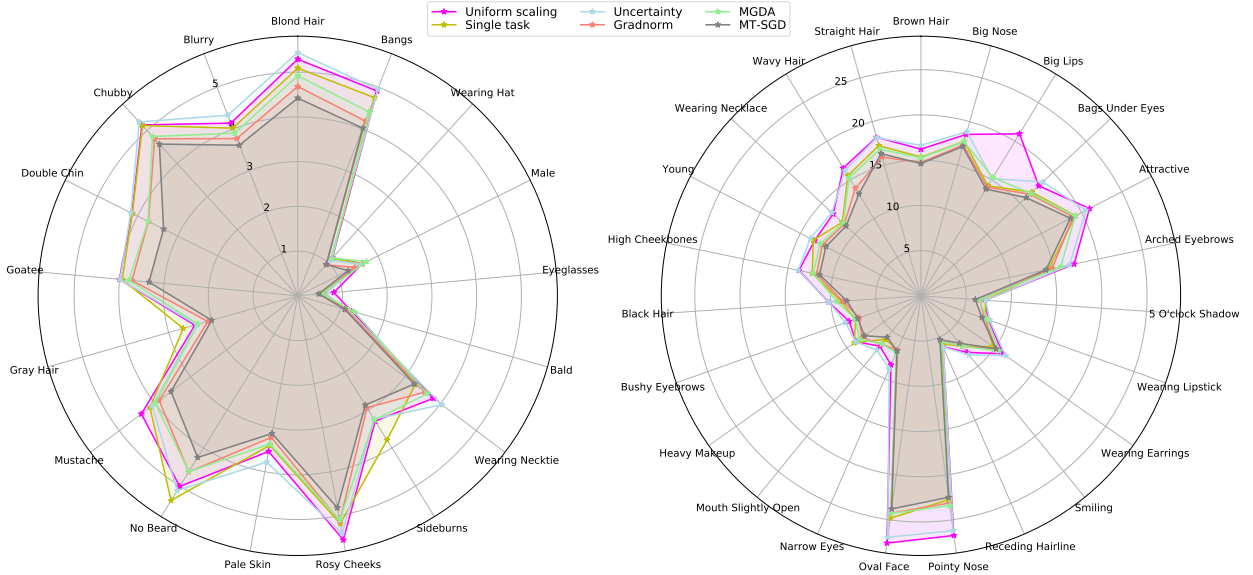


Figure 10: Radar charts of prediction error on CelebA [18] for each individual binary classification task. We divide attributes into two sets: easy tasks on the left, difficult tasks on the right, as in [27].

Table 5: Average performance (lower is better) of each target attribute for all baselines. We use the **bold** font to highlight the best-obtained score in each task.

Attribute	Uniform scaling	Single task	Uncertainty	Gradnorm	MGDA	MT-SGD
5 O'clock Shadow	7.11	7.16	7.18	6.54	6.47	6.03
Arched Eyebrows	17.30	14.38	16.77	14.80	15.80	14.11
Attractive	20.99	19.25	20.56	18.97	19.21	18.62
Bags Under Eyes	17.82	16.79	18.45	16.47	16.60	15.91
Bald	1.25	1.20	1.17	1.13	1.32	1.09
Bangs	4.91	4.75	4.95	4.19	4.41	4.02
Big Lips	20.97	14.24	15.17	14.07	15.32	13.82
Big Nose	18.53	17.74	18.84	17.33	17.70	17.14
Black Hair	10.22	8.87	10.19	8.67	9.31	8.22
Blond Hair	5.29	5.09	5.44	4.68	4.92	4.42
Blurry	4.14	4.02	4.33	3.77	3.90	3.61
Brown Hair	16.22	15.34	16.64	14.73	15.27	14.63
Bushy Eyebrows	8.42	7.68	8.85	7.23	7.69	7.42
Chubby	5.17	5.15	5.26	4.75	4.82	4.59
Double Chin	4.14	4.13	4.17	3.73	3.74	3.35
Eyeglasses	0.81	0.52	0.62	0.56	0.54	0.47
Goatee	4.00	3.94	3.99	3.72	3.79	3.34
Gray Hair	2.39	2.66	2.35	2.09	2.32	2.00
Heavy Makeup	8.79	9.01	8.84	8.00	8.29	7.65
High Cheekbones	13.78	12.27	13.86	11.79	12.18	11.45
Male	1.61	1.61	1.58	1.42	1.72	1.26
Mouth Slightly Open	7.18	6.20	7.73	6.91	6.86	5.91
Mustache	4.38	4.14	4.08	3.88	3.99	3.55
Narrow Eyes	8.32	6.57	8.80	6.54	6.88	6.64
No Beard	5.01	5.38	5.12	4.63	4.62	4.25
Oval Face	27.59	24.82	26.94	24.26	24.28	23.78
Pale Skin	3.54	3.40	3.78	3.22	3.37	3.13
Pointy Nose	26.74	22.74	26.21	23.12	23.41	22.48
Receding Hairline	6.14	5.82	6.17	5.43	5.52	5.28
Rosy Cheeks	5.55	5.18	5.40	5.13	5.10	4.82
Sideburns	3.29	3.79	3.24	2.94	3.26	2.87
Smiling	8.05	7.18	8.40	7.21	7.19	6.74
Straight Hair	18.21	17.25	18.15	15.93	16.82	16.32
Wavy Hair	16.53	15.55	16.19	13.93	15.28	13.19
Wearing Earrings	11.12	9.76	11.46	10.17	10.57	10.17
Wearing Hat	1.15	1.13	1.08	0.94	1.14	0.95
Wearing Lipstick	7.91	7.56	8.06	7.47	7.76	7.15
Wearing Necklace	13.27	11.90	13.47	11.61	11.75	11.32
Wearing Necktie	3.80	3.29	4.04	3.57	3.63	3.27
Young	13.25	13.40	13.78	12.26	12.53	11.83
Average	9.62	8.77	9.53	8.44	8.73	8.17

References

- [1] Mark Anderson and Carlos Gómez-Rodríguez. A modest Pareto optimisation analysis of dependency parsers in 2021. In *Proceedings of the 17th International Conference on Parsing Technologies and the IWPT 2021 Shared Task on Parsing into Enhanced Universal Dependencies (IWPT 2021)*, pages 119–130, Online, August 2021. Association for Computational Linguistics.
- [2] Christopher M. Bishop. *Pattern Recognition and Machine Learning (Information Science and Statistics)*. Springer-Verlag, Berlin, Heidelberg, 2006.
- [3] Glenn W Brier et al. Verification of forecasts expressed in terms of probability. *Monthly weather review*, 78(1):1–3, 1950.
- [4] Zhao Chen, Vijay Badrinarayanan, Chen-Yu Lee, and Andrew Rabinovich. Gradnorm: Gradient normalization for adaptive loss balancing in deep multitask networks. In *International Conference on Machine Learning*, pages 794–803. PMLR, 2018.
- [5] Zhengyu Chen, Jixie Ge, Heshen Zhan, Siteng Huang, and Donglin Wang. Pareto self-supervised training for few-shot learning. In *Proceedings of the IEEE/CVF Conference on Computer Vision and Pattern Recognition*, pages 13663–13672, 2021.
- [6] Sumanth Chennupati, Mohammad Mahdi Kamani, Zhongwei Cheng, and Lin Chen. Adaptive distillation: Aggregating knowledge from multiple paths for efficient distillation. *arXiv preprint arXiv:2110.09674*, 2021.
- [7] A Philip Dawid. The well-calibrated bayesian. *Journal of the American Statistical Association*, 77(379):605–610, 1982.
- [8] Jean-Antoine Désidéri. Multiple-gradient descent algorithm (mgda) for multiobjective optimization. *Comptes Rendus Mathématique*, 350(5-6):313–318, 2012.
- [9] Shangchen Du, Shan You, Xiaojie Li, Jianlong Wu, Fei Wang, Chen Qian, and Changshui Zhang. Agree to disagree: Adaptive ensemble knowledge distillation in gradient space. *advances in neural information processing systems*, 33:12345–12355, 2020.
- [10] Shaona Ghosh, Chris Lovell, and Steve R Gunn. Towards pareto descent directions in sampling experts for multiple tasks in an on-line learning paradigm. In *2013 AAAI Spring Symposium Series*, 2013.
- [11] Kaiming He, Xiangyu Zhang, Shaoqing Ren, and Jian Sun. Deep residual learning for image recognition. In *Proceedings of the IEEE conference on computer vision and pattern recognition*, pages 770–778, 2016.
- [12] Alex Kendall, Yarin Gal, and Roberto Cipolla. Multi-task learning using uncertainty to weigh losses for scene geometry and semantics. In *Proceedings of the IEEE conference on computer vision and pattern recognition*, pages 7482–7491, 2018.
- [13] Diederik P Kingma and Jimmy Ba. Adam: A method for stochastic optimization. *Proceedings of the International Conference on Learning Representations*, 2014.

- [14] Yann LeCun, Léon Bottou, Yoshua Bengio, and Patrick Haffner. Gradient-based learning applied to document recognition. *Proceedings of the IEEE*, 86(11):2278–2324, 1998.
- [15] Xi Lin, Hui-Ling Zhen, Zhenhua Li, Qing-Fu Zhang, and Sam Kwong. Pareto multi-task learning. *Advances in neural information processing systems*, 32, 2019.
- [16] Qiang Liu and Dilin Wang. Stein variational gradient descent: A general purpose bayesian inference algorithm. *Advances in neural information processing systems*, 29, 2016.
- [17] Xingchao Liu, Xin Tong, and Qiang Liu. Profiling pareto front with multi-objective stein variational gradient descent. *Advances in Neural Information Processing Systems*, 34, 2021.
- [18] Ziwei Liu, Ping Luo, Xiaogang Wang, and Xiaoou Tang. Deep learning face attributes in the wild. In *Proceedings of the IEEE international conference on computer vision*, pages 3730–3738, 2015.
- [19] Debabrata Mahapatra and Vaibhav Rajan. Multi-task learning with user preferences: Gradient descent with controlled ascent in pareto optimization. In *International Conference on Machine Learning*, pages 6597–6607. PMLR, 2020.
- [20] Kevin P. Murphy. *Probabilistic Machine Learning: An introduction*. MIT Press, 2022.
- [21] Mahdi Pakdaman Naeini, Gregory Cooper, and Milos Hauskrecht. Obtaining well calibrated probabilities using bayesian binning. In *Twenty-Ninth AAAI Conference on Artificial Intelligence*, 2015.
- [22] Aviv Navon, Aviv Shamsian, Ethan Fetaya, and Gal Chechik. Learning the pareto front with hypernetworks. In *International Conference on Learning Representations*, 2021.
- [23] Yaniv Ovadia, Emily Fertig, Jie Ren, Zachary Nado, David Sculley, Sebastian Nowozin, Joshua Dillon, Balaji Lakshminarayanan, and Jasper Snoek. Can you trust your model’s uncertainty? evaluating predictive uncertainty under dataset shift. *Advances in neural information processing systems*, 32, 2019.
- [24] Simone Parisi, Matteo Pirotta, Nicola Smacchia, Luca Bascetta, and Marcello Restelli. Policy gradient approaches for multi-objective sequential decision making. In *2014 International Joint Conference on Neural Networks (IJCNN)*, pages 2323–2330. IEEE, 2014.
- [25] Matteo Pirotta and Marcello Restelli. Inverse reinforcement learning through policy gradient minimization. In *Thirtieth AAAI Conference on Artificial Intelligence*, 2016.
- [26] Sara Sabour, Nicholas Frosst, and Geoffrey E Hinton. Dynamic routing between capsules. In I. Guyon, U. Von Luxburg, S. Bengio, H. Wallach, R. Fergus, S. Vishwanathan, and R. Garnett, editors, *Advances in Neural Information Processing Systems*, volume 30. Curran Associates, Inc., 2017.
- [27] Ozan Sener and Vladlen Koltun. Multi-task learning as multi-objective optimization. *Advances in neural information processing systems*, 31, 2018.
- [28] Sethu Vijayakumar, Aaron D’souza, Tomohiro Shibata, Jörg Conradt, and Stefan Schaal. Statistical learning for humanoid robots. *Autonomous Robots*, 12(1):55–69, 2002.

- [29] Martin J. Wainwright and Michael I. Jordan. Graphical models, exponential families, and variational inference. *Foundations and Trends in Machine Learning*, 1(1–2):1–305, 2008.
- [30] Max Welling and Yee W Teh. Bayesian learning via stochastic gradient langevin dynamics. In *Proceedings of the 28th international conference on machine learning (ICML-11)*, pages 681–688. Citeseer, 2011.
- [31] Han Xiao, Kashif Rasul, and Roland Vollgraf. Fashion-mnist: a novel image dataset for benchmarking machine learning algorithms. *arXiv preprint arXiv:1708.07747*, 2017.
- [32] Feiyang Ye, Baijiong Lin, Zhixiong Yue, Pengxin Guo, Qiao Xiao, and Yu Zhang. Multi-objective meta learning. *Advances in Neural Information Processing Systems*, 34, 2021.
- [33] Eckart Zitzler, Kalyanmoy Deb, and Lothar Thiele. Comparison of multiobjective evolutionary algorithms: Empirical results. *Evolutionary computation*, 8(2):173–195, 2000.